

Multi-Higgs Boson Probes of the Dark Sector

Marvin Flores^{1,2}, Christian Gross³, Jong Soo Kim⁴,
Oleg Lebedev⁵ and Subhadeep Mondal⁵

¹ *School of Physics, University of the Witwatersrand,
Johannesburg, South Africa*

² *National Institute of Physics, University of the Philippines,
Diliman, Quezon City, Philippines*

³ *Dipartimento di Fisica dell'Università di Pisa and INFN, Sezione di Pisa,
IT-56127 Pisa, Italy*

⁴ *National Institute for Theoretical Physics and School of Physics,
University of the Witwatersrand, Johannesburg, South Africa*

⁵ *Department of Physics and Helsinki Institute of Physics,
Gustaf Hållströmin katu 2a, FI-00014 Helsinki, Finland*

Abstract

We consider dark sectors with spontaneously broken gauge symmetries, where cascade decays of the dark sector fields naturally produce multi-Higgs boson final states along with dark matter. Our study focuses on two and three Higgs boson final states with missing energy using a multivariate analysis with Boosted Decision Trees. We find that the di-Higgs boson channel is quite promising for the $\bar{b}b + \gamma\gamma$ and $\bar{b}b + \bar{\ell}\ell$ decay modes. The tri-Higgs boson final state with missing energy, on the other hand, appears to be beyond the reach of the LHC in analogous channels. This may change when fully hadronic Higgs boson decays are considered.

Contents

1	Introduction	1
2	Motivation: multi-Higgs states and missing energy from dark gauge sectors	2
2.1	Dark Higgsed gauge sectors	2
2.2	Simplified model	3
3	LHC search for di-Higgs production with missing energy	6
3.1	$2b + 2\gamma + \cancel{E}_T$ in the final state	6
3.2	Problems with the cut-based analysis	7
3.3	Multivariate analysis	10
3.3.1	Results	11
3.4	Multivariate analysis for $2b$ -jets + $2\ell + \cancel{E}_T$ in the final state	13
3.4.1	Results	13
4	LHC search for a tri-Higgs and dark matter final state	15
4.1	Multivariate analysis for $\geq 3b$ -jets + $2\ell + \cancel{E}_T$ in the final state	15
5	Summary and Conclusions	17

1 Introduction

The scalar sector of the Standard Model (SM) remains relatively little explored compared to the gauge sector. In particular, no Higgs boson self-interaction has been measured. It is a well motivated and experimentally viable possibility that the Higgs field plays the role of a portal into the hidden sector which may contain dark matter and possibly other cosmologically relevant fields [1–3]. Exploring this portal requires Higgs coupling measurements as well as a search for extra states. The Higgs self-coupling can be determined via Higgs boson pair production – one of the central objectives of the future (HL)-LHC searches, cf. eg. [4] for a recent summary. Higgs portal dark matter can manifest itself in di-Higgs or multi-Higgs final states with large missing energy, which appears due to emission of undetected dark matter. Analogous signals arise in a multitude of New Physics models as studied in [5–20]. LHC searches for di-Higgs + \cancel{E}_T have been presented in [21–23].

Within a similar framework, a study of di-Higgs + \cancel{E}_T production with the $4b + \cancel{E}_T$ final state has been performed in [24]. It utilises a jet substructure technique to reconstruct the boosted Higgs bosons. While for heavy dark states this method is efficient, in the intermediate mass range (below 700 GeV or so) it is less reliable. In our work, we consider both 2 and 3 Higgs final states, which subsequently decay into $b\bar{b}$, $\gamma\gamma$ and WW . These have the advantage of being cleaner channels with a lower background. Instead of using a traditional cut-based analysis, we employ (as done for $4b + \cancel{E}_T$ in [24]) a multivariate technique with Boosted Decision Trees which leads to much better sensitivity to New Physics. Further probes of the model are provided by monojet + \cancel{E}_T searches [25]. The analysis of [25] is based on rectangular cuts and as such leads to lower sensitivity than the present study does.

To set the framework for our study, we introduce a simplified model in which cascade decays of heavier states produce dark matter and the Higgses. This model is

motivated by non-Abelian gauged hidden sectors in which gauge symmetry is broken completely by VEVs of a minimal set of dark Higgs multiplets [26]. Such models automatically lead to stable dark matter which consists of a subset of gauge fields (and possibly extra scalars). Smaller groups like U(1) and SU(2) [27, 28] do not allow for the needed cascade decays, while SU(3) and larger groups have all the necessary features. Further options, e.g. when part of the gauge group condenses, have been explored in [29, 30].

This paper is structured as follows. In Section 2, we motivate our study and introduce the simplified model. In Section 3, we perform an LHC study of the di-Higgs final state with missing energy using multivariate analysis with Boosted Decision Trees and present the resulting sensitivity to model parameters. In Section 4, our findings on the tri-Higgs final state with missing energy are summarized. Section 5 concludes our study.

2 Motivation: multi-Higgs states and missing energy from dark gauge sectors

2.1 Dark Higgsed gauge sectors

The presence of stable states which can play the role of dark matter is a common feature of dark sectors with spontaneously broken gauge symmetry. In particular, breaking SU(N) completely with the minimal number of dark Higgs fields automatically leads to stable dark matter. To be specific, let us briefly summarize the main relevant features of the SU(3) example [26] (see also [31, 32]). The set-up contains two dark Higgs triplets ϕ_i to break the symmetry completely.¹ The Lagrangian is $\mathcal{L}_{\text{SM}} + \mathcal{L}_{\text{portal}} + \mathcal{L}_{\text{hidden}}$, where

$$-\mathcal{L}_{\text{SM}} \supset V_{\text{SM}} = \frac{\lambda}{2}|H|^4 + m^2|H|^2, \quad (1a)$$

$$-\mathcal{L}_{\text{portal}} = |H|^2 \left(\sum_{i=1}^2 \lambda_{Hi} |\phi_i|^2 - \left(\lambda_{H12} \phi_1^\dagger \phi_2 + \text{h.c.} \right) \right), \quad (1b)$$

$$\mathcal{L}_{\text{hidden}} = -\frac{1}{2} \text{tr}\{G_{\mu\nu} G^{\mu\nu}\} + \sum_{i=1}^2 |D_\mu \phi_i|^2 - V_{\text{hidden}}. \quad (1c)$$

Here, $G_{\mu\nu} = \partial_\mu A_\nu - \partial_\nu A_\mu + i\tilde{g}[A_\mu, A_\nu]$ is the field strength tensor of the SU(3) gauge fields A_μ^a with gauge coupling \tilde{g} , $D_\mu \phi_i = \partial_\mu \phi_i + i\tilde{g} A_\mu \phi_i$, and H is the Higgs doublet, which in the unitary gauge can be written as $H^T = (0, v + h)/\sqrt{2}$. The potential for the dark Higgses is given by

$$\begin{aligned} V_{\text{hidden}}(\phi_1, \phi_2) = & m_{11}^2 |\phi_1|^2 + m_{22}^2 |\phi_2|^2 - (m_{12}^2 \phi_1^\dagger \phi_2 + \text{h.c.}) \\ & + \frac{\lambda_1}{2} |\phi_1|^4 + \frac{\lambda_2}{2} |\phi_2|^4 + \lambda_3 |\phi_1|^2 |\phi_2|^2 + \lambda_4 |\phi_1^\dagger \phi_2|^2 \\ & + \left[\frac{\lambda_5}{2} (\phi_1^\dagger \phi_2)^2 + \lambda_6 |\phi_1|^2 (\phi_1^\dagger \phi_2) + \lambda_7 |\phi_2|^2 (\phi_1^\dagger \phi_2) + \text{h.c.} \right]. \end{aligned} \quad (2)$$

¹This is the minimal scalar field content needed to break SU(3) completely. With fewer scalars, part of the gauge group would remain unbroken and may eventually condense, leading to different phenomenology, cf. [29, 30].

fields	$Z_2 \times Z'_2$
$h, \varphi^1, \varphi^2, \varphi^3, A_\mu^7$	$(+, +)$
A_μ^2, A_μ^5	$(-, +)$
A_μ^1, A_μ^4	$(-, -)$
$\varphi^4, A_\mu^3, A_\mu^6, A_\mu^8$	$(+, -)$

Table 1: $Z_2 \times Z'_2$ parities of the scalars and dark gauge bosons.

In the unitary gauge, ϕ_1, ϕ_2 can be written as

$$\phi_1 = \frac{1}{\sqrt{2}} \begin{pmatrix} 0 \\ 0 \\ v_1 + \varphi_1 \end{pmatrix}, \quad \phi_2 = \frac{1}{\sqrt{2}} \begin{pmatrix} 0 \\ v_2 + \varphi_2 \\ v_3 + \varphi_3 + i(v_4 + \varphi_4) \end{pmatrix}, \quad (3)$$

where the v_i are real VEVs and φ_i are real scalar fields.

For simplicity, we assume an unbroken CP symmetry in the scalar sector, i.e. we assume that the couplings are real and $v_4 = 0$.² As explained in [26, 34], the model then has an unbroken $U(1) \times Z'_2$ global symmetry. Its $Z_2 \times Z'_2$ subgroup leads to stability of multicomponent DM. The parities of the fields under $Z_2 \times Z'_2$ transformations are summarized in Table 1.

The lightest states with non-trivial parities cannot decay to the Standard Model particles and are viable DM candidates. The hidden vector and scalar fields can mix with other fields of the same $Z_2 \times Z'_2$ parity.

In this example, A_μ^{1-3} and φ^4 play the role of dark matter. The other vectors A_μ^{4-8} are heavier and decay into A_μ^{1-3} with scalar emission. The scalar couplings to the vectors depend on the VEVs of the triplets as well as their mixing with the SM Higgs. The CP-even scalars are all expected to mix and their mass eigenstates include the 125 GeV Higgs h , a heavier scalar H and two more heavy scalars which play no significant role in our discussion. Given that H -emission is often kinematically forbidden, cascade decays of the heavy states naturally produce multi-Higgs h signals.

2.2 Simplified model

In our study, only main features of this set-up play a role. Hence, it is convenient to introduce a simplified model which inherits salient features of the Higgs portal framework. Consider an extension of the SM by three fields: a Higgs-like scalar H with mass m_H , a stable vector field A_L with mass m_{A_L} and a heavier unstable vector field A_H with mass m_{A_H} . Dark matter is assumed to be composed of A_L , while the 125 GeV Higgs h and the heavier Higgs H are mixtures of the SM Higgs doublet and the hidden sector singlet characterized by the mixing angle θ .

The interactions of the prototype fields are listed in [26]. The result depends on which of the triplets the SM Higgs mixes with predominantly. For our purposes, it is convenient to parametrize the couplings in terms of the mixing angles as follows. The couplings of h, H to SM matter and SM gauge fields are given by

$$\mathcal{L} \supset (h \cos \theta + H \sin \theta) \frac{1}{v} \left[2m_W^2 W_\mu^+ W^{\mu-} + m_Z^2 Z_\mu Z^\mu - \sum_f m_f \bar{f} f \right], \quad (4)$$

²If this assumption is relaxed, the model still has dark matter which consists of a subset of stable states considered here [33].

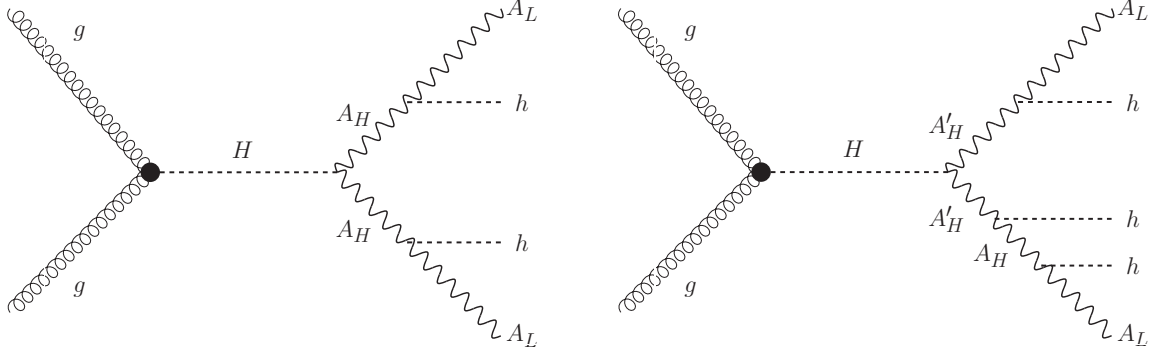


Figure 1: Left: $hh + \cancel{E}_T$ production. Right: $hhh + \cancel{E}_T$ production.

while the couplings of h, H to A_L, A_H are given by

$$\mathcal{L} \supset (-h \sin \theta + H \cos \theta) \frac{\tilde{g}}{2} [\cos \delta m_{A_L} (A_L^\mu)^2 + \sin \delta m_{A_H} (A_H^\mu)^2] . \quad (5)$$

In addition to the masses, the New Physics parameters are: the dark gauge coupling \tilde{g} , the Higgs mixing angle θ and an angle δ that sets the relative strength of the scalar coupling to the dark vectors.³ Further relevant couplings include the terms

$$\mathcal{L} \supset -\kappa_{112} \frac{v}{2} H h^2 - \sigma (A_L)_\mu A_H^\mu h . \quad (6)$$

Here κ_{112} is not fixed by the other model parameters, so that we can take $\text{BR}(H \rightarrow hh)$ to be a free variable. The σ -term, which is also a free parameter within the simplified model, accounts for decay of the heavy gauge boson into dark matter and SM states.

The di-Higgs + \cancel{E}_T final state is generated through the diagram in Fig. 1, left. We consider the regime where H is produced on-shell and decays into a pair of A_H with a significant branching fraction. These subsequently decay into A_L 's and h 's as long as kinematically allowed, while the A_L pair escapes undetected thereby producing the missing energy signal.

In the simplest model, $\text{BR}(A_H \rightarrow A_L + h) \simeq 100\%$ for $m_{A_H} > m_{A_L} + m_h$. On the other hand, $\text{BR}(H \rightarrow A_H A_H)$ varies. The partial width for the H decay into SM fermions and SM vector bosons is given by

$$\Gamma(H \rightarrow f \bar{f}, ZZ, W^+ W^-) = \sin^2 \theta \times \Gamma_{\text{SM}}|_{m_h \rightarrow m_H} . \quad (7)$$

The partial widths for the H decay to hidden vectors are given by

$$\Gamma(H \rightarrow A_L A_L) = \frac{\tilde{g}^2 \cos^2 \theta \cos^2 \delta m_H^3}{128 \pi m_{A_L}^2} f(x_L) , \quad (8a)$$

$$\Gamma(H \rightarrow A_H A_H) = \frac{\tilde{g}^2 \cos^2 \theta \sin^2 \delta m_H^3}{128 \pi m_{A_H}^2} f(x_H) , \quad (8b)$$

where $x_{L/H} \equiv 4m_{A_{L/H}}^2/m_H^2$ and $f(x) = (1 - x + 3x^2/4) \sqrt{1 - x}$. Fig. 2 shows the variation of $\text{BR}(H \rightarrow A_H A_H)$ with m_{A_H} and $\cos \delta$. The other parameters are set to

³Within the UV complete model of the previous subsection, $\sin \delta$ depends on the composition of the heavy Higgs H in terms of the CP even dark scalars.

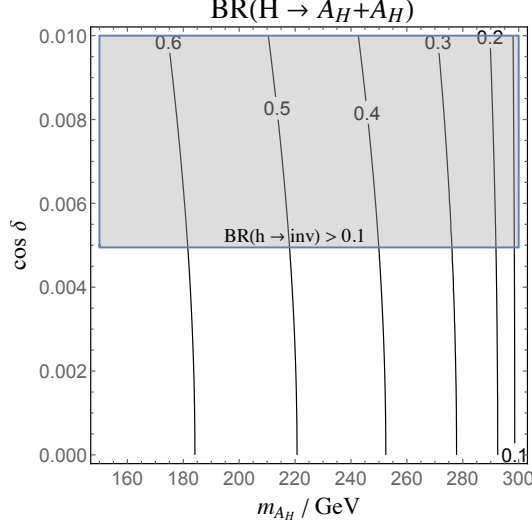


Figure 2: Branching ratio for the heavy Higgs decay to heavier dark bosons $H \rightarrow A_H A_H$. Here $\sin \theta = 0.3$, $\tilde{g} = 2$, $m_H = 600$ GeV, $m_{A_L} = 10$ GeV, $\text{BR}(H \rightarrow hh) = 0.2$. The shaded region is excluded by $\text{BR}(h \rightarrow \text{inv}) > 0.1$.

$\sin \theta = 0.3$, $\tilde{g} = 2$, $m_H = 600$ GeV, $m_{A_L} = 10$ GeV and $\text{BR}(H \rightarrow hh)$ is kept fixed at 0.2. This choice is motivated by having a sizeable production cross section for H : both $\sin \theta$ and \tilde{g} should be substantial, while H should not be too heavy. We see that $\cos \delta$ is required to be small in order to get a significant $\text{BR}(H \rightarrow A_H A_H)$. A large portion of parameter space is excluded by the invisible h -decay constraint $\text{BR}(h \rightarrow \text{inv}) < 0.1$, which also forces $\cos \delta \ll 1$. More precisely, the relevant bound is that on the signal strength μ of the 125 GeV Higgs which constrains a combination of $\sin \theta$ and the invisible decay BR (see e.g. the discussion in [35]). Given the fluctuations in the experimental values of μ , we take the resulting constraint on $h \rightarrow \text{inv}$ to be $\text{BR}(h \rightarrow \text{inv}) < 0.1$. The precise value of this bound does not affect our results. In the SU(3) model, the smallness of $\cos \delta$ can be attributed to the Higgs mixing predominantly with one of the triplets, namely ϕ_1 , such that H has a large ϕ_1 component (see Table 3 of [26].) Finally, we note that the chosen values of $\sin \theta$ and m_H are consistent with both the LHC and electroweak precision measurements [35, 36], although a stronger bound on $\sin \theta$ from the W mass alone has been quoted in Ref. [37].

In this work, we are being agnostic as to the DM production mechanism and do not impose a constraint on the thermal DM annihilation cross-section.⁴ On the other hand, the direct DM detection cross-section is automatically suppressed: the h -mediated contribution is small due to $\cos^2 \delta \ll 1$, while the H -mediated contribution is suppressed by $\sin^2 \theta$ and m_H^4 . Thus, in what follows we may focus on the collider aspects of the model as long as the parameter values are in the ballpark of those considered in this section.

The simplified model can be added a layer of complexity by including an extra heavy gauge boson A'_H . Indeed, dark sectors with the symmetry group larger than SU(2) contain multiple heavy bosons with different masses. The relevant couplings take the form

$$\mathcal{L} \supset \lambda_{abi} (A_a)_\mu (A_b)^\mu \Phi_i, \quad (9)$$

⁴The thermal DM analysis for the SU(3) model has been performed in [26].

where $A_a = A'_H, A_H, A_L$ and $\Phi_i = h, H$. Depending on the couplings λ_{abi} and masses, H may predominantly decay into a pair of A'_H , which then decay into A_H and A_L with h -emission. This can lead, for example, to a $3h$ and dark matter final state as shown in Fig. 1, right. Such exotic processes may provide an additional handle on the dark sector properties.

3 LHC search for di-Higgs production with missing energy

3.1 $2b + 2\gamma + \cancel{E}_T$ in the final state

Certain aspects of collider phenomenology of related models have been studied before [6, 24, 25, 38–42] through different production channels. In this work, we focus on the heavy CP-even scalar (H) production through gluon fusion, which subsequently decays via the hidden sector vector fields into the 125 GeV Higgs bosons (h) along with two dark matter particles. This can result in various final states depending on the decay mode of the 125 GeV Higgs boson. The dominant decay of the Higgs to $b\bar{b}$ has been studied extensively in [24]. However, such a multi- b -jet final state is plagued with hadronic backgrounds and one needs a very clear understanding of the W +jets and QCD backgrounds at high luminosity in order to isolate the signal events. Using the jet substructure technique to reconstruct the Higgs bosons is an efficient tool for a heavy H , while in the mass range of interest to us it is less reliable.

Instead, we explore a cleaner channel where one of the 125 GeV Higgs bosons decays into a pair of photons. The photon identification efficiency is quite good and even though the corresponding branching ratio is small, an enhanced cut efficiency makes this channel a significant one. Thus, our signal region consists of two b -jets, two photons and large transverse missing energy. The LHC collaborations have studied the two b -jets + 2 photons signal region quite extensively in the context of BSM Higgs searches [43]. However, this does not include large missing energy which we use as an additional feature to suppress the SM background.

The dominant SM background to the signal arises from the $t\bar{t}h$, $b\bar{b}h$, Zh , $\gamma\gamma$ +jets, $t\bar{t}\gamma\gamma$, $b\bar{b}\gamma\gamma$ and $ZZ\gamma\gamma$ production. In addition, there are contributions from $b\bar{b}\gamma$ +jets and $b\bar{b}$ +jets with the jet(s) being mistagged as photon(s), which can be important due to pile-up at the LHC at high luminosity. Although the mistagging probability is small, of order 0.1% [44], the resultant background cross-section may not be negligible given the large production cross-section for these two processes. We have simulated all of the above processes along with our signal for some representative benchmark points at the 14 TeV LHC. The parton level events have been generated using MadGraph5 [45, 46]. We use the NNPDF parton distribution function [47, 48] for our computation. These events are then passed through PYTHIA8 [49, 50] for decay, showering and hadronisation. For processes with additional jets at the parton level, MLM matching [51, 52] was performed through the MadGraph5-PYTHIA8 interface. The complete event information is further passed through Delphes3 [53–55] for detector simulation. The jets are constructed via FastJet [56] following the anti-kt [57] algorithm with radius parameter $R = 0.4$.

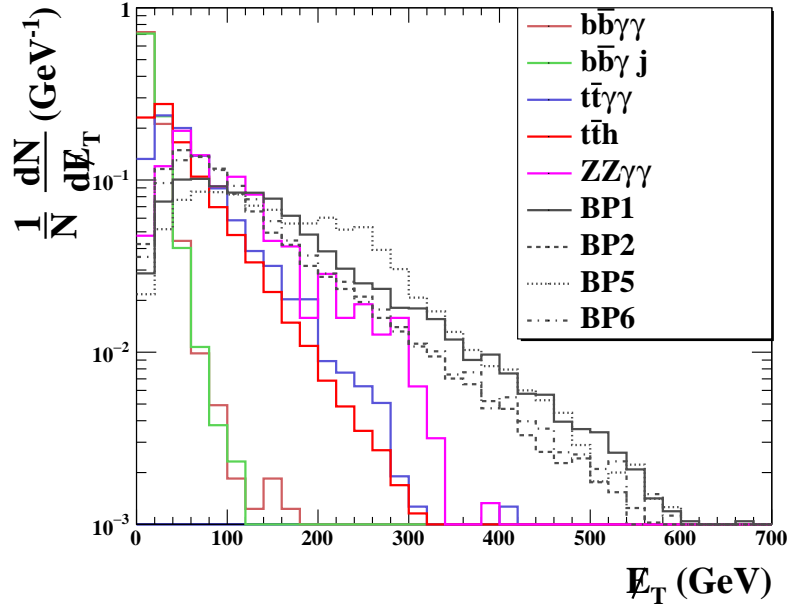


Figure 3: \cancel{E}_T distribution for some of the benchmark points and background processes for the final state $2b + 2\gamma + \cancel{E}_T$.

3.2 Problems with the cut-based analysis

In our scenario, the two b -jets and two photons in the final state arise from on-shell Higgs decays. In addition, the final state contains two dark matter particles which contribute to the missing transverse energy. In order to tag the b -jets, we have used a tagging efficiency which depends on the b transverse momentum, $0.80 \times \tanh(0.003 \times p_T) \frac{30}{(1+0.086 \times p_T)}$ as provided by the ATLAS collaboration [58]. We have also considered the possibility of a light jet being mistagged as a b -jet. The mistagging probability is largest for the c -jets: $0.20 \times \tanh(0.02 \times p_T) \frac{1}{(1+0.0034 \times p_T)}$ and much lower for the other light jets: $0.002 + 7.3 \times 10^{-6} \times p_T$ [58]. In order to tag isolated charged leptons and photons, we impose the requirements $p_T > 20$ GeV and $|\eta| < 2.5$, where η is the pseudorapidity. We further ensure that all the leptons are well separated among themselves with $\Delta R_{\ell\ell} > 0.2$ and also from other particles, $\Delta R_{\ell x} > 0.4$, where x can be either photons or jets. Furthermore, the transverse energy deposited by the hadrons within a cone of $\Delta R \leq 0.2$ around the lepton is required to be less than $0.2 \times p_T^\ell$. Similar ΔR and hadronic energy deposition criteria are also imposed on the photons for them to be considered isolated. A jet-jet separation $\Delta R_{jj} > 0.4$ is also imposed. We use the following kinematic cuts to achieve a good signal to background ratio:⁵

- **C1:** The final state must contain two b -jets with $p_T^b > 25$ GeV and two photons. Pseudorapidity of both the b -jets and the photons must lie within $|\eta| < 2.5$. There should be no isolated charged leptons in the final state.
- **C2:** The transverse missing energy \cancel{E}_T must be larger than 120 GeV. This cut is particularly useful to reduce background contributions from the channels with no direct source of missing energy, namely, $b\bar{b}h$, Zh , $\gamma\gamma + \text{jets}$, $b\bar{b}\gamma\gamma$, $b\bar{b}\gamma + \text{jets}$ and $b\bar{b} + \text{jets}$. For all these channels, \cancel{E}_T in the final state arises from

⁵Many of these cuts are borrowed from the CMS analysis [43].

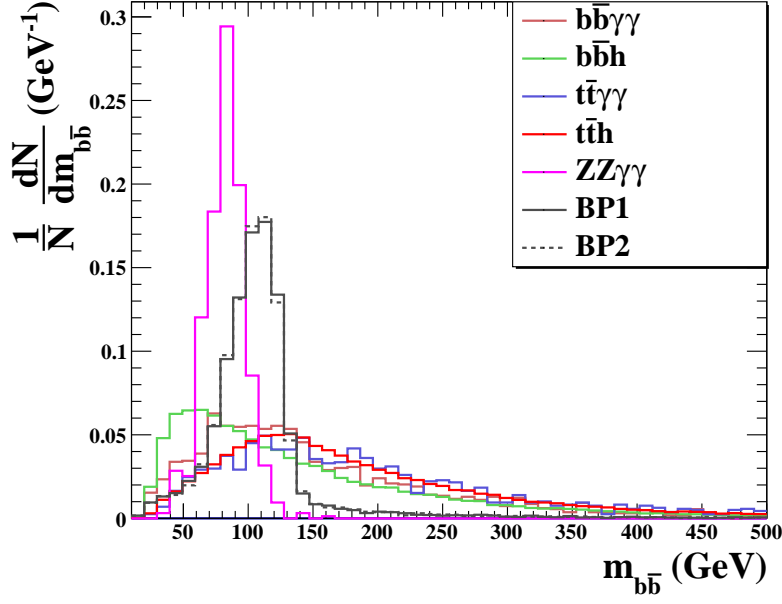


Figure 4: $m_{b\bar{b}}$ distribution for some of the benchmark points and background processes for the final state $2b + 2\gamma + \cancel{E}_T$.

mismeasurement of the jet transverse momenta. Its distribution is likely to be much softer than that of the channels like $t\bar{t}h$, $t\bar{t}\gamma\gamma$, and $ZZ\gamma\gamma$ as shown in Fig. 3.

- **C3:** Invariant mass of the b -jet pair must lie within a 20 GeV window of the 125 GeV Higgs, $|m_{b\bar{b}} - 125 \text{ GeV}| < 20 \text{ GeV}$. The background b -jets are either hard produced or arise from top quark or Z boson decay. Hence the invariant mass of the b -jet pairs is distributed over a wide range in most cases, whereas for Zh and $ZZ\gamma\gamma$ it peaks around the Z boson mass as can be seen from Fig. 4. Thus, the cut on the $b\bar{b}$ invariant mass reduces the background contribution drastically.
- **C4:** Effective mass $m_{\text{eff}} = \sum_i p_T^{b_i} + \sum_i p_T^{\gamma_i} + \cancel{E}_T$ must be larger than 800 GeV. For the signal events, this quantity is normally larger than that for the background channels like Zh , $b\bar{b}h$. This cut also helps to reduce background contributions from soft b -jets and photons in processes like $b\bar{b}\gamma\gamma$, $b\bar{b}\gamma + \text{jets}$ and $b\bar{b} + \text{jets}$.
- **C5:** Invariant mass of the photon pair must lie within a 5 GeV window of the 125 GeV Higgs, $|m_{\gamma\gamma} - 125 \text{ GeV}| < 5 \text{ GeV}$. The Higgs mass reconstruction from the photon pair is much more precise than that from the b -jets due to the better photon momentum resolution, thus allowing for efficient discrimination against many of the background channels (except for $t\bar{t}h$, $b\bar{b}h$ and Zh). The corresponding kinematic distribution for some of the signal and background processes is shown in Fig. 5.
- **C6:** Angular separation between the $b\bar{b}$ pair and the photon pair must be large, $\Delta\phi(b\bar{b}, \gamma\gamma) > 2.0$. Since the two Higgs bosons are radiated from two different legs in the production process, it is expected that the resultant b -jet pair and the γ pair will be well separated in the final state. This is not the case for some of the background processes, especially those where all the b -jets and photons are hard produced, like $b\bar{b}\gamma\gamma$, etc. The two b -jets can also arise from decays of

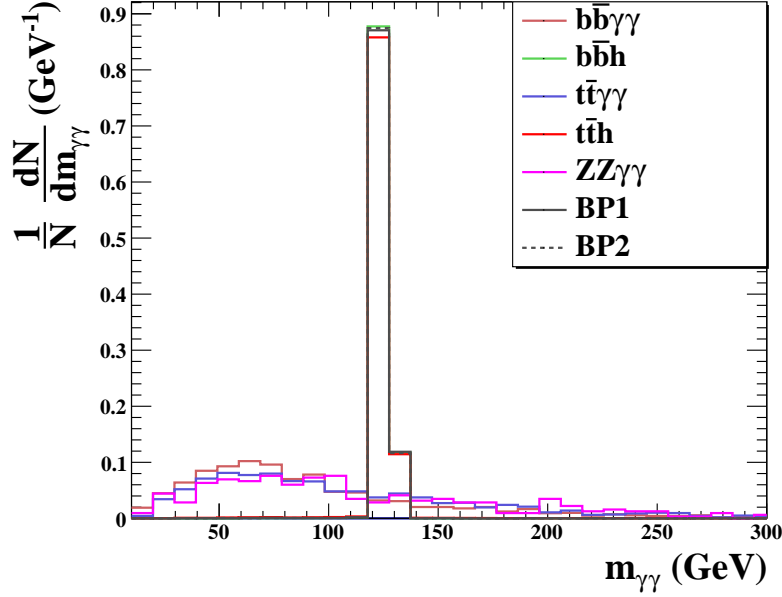


Figure 5: Distribution of $m_{\gamma\gamma}$ for some sample benchmark points and background processes for the final state $2b + 2\gamma + \cancel{E}_T$.

two different mother particles, as in $t\bar{t}\gamma\gamma$, in which case the combined $b\bar{b}$ system may not be well separated from the $\gamma\gamma$ system.

- **C7:** $\frac{p_T^{\gamma 1}}{m_{\gamma\gamma}} > \frac{1}{3}$ and $\frac{p_T^{\gamma 2}}{m_{\gamma\gamma}} > \frac{1}{4}$. This eliminates some of the distortions in the low end of the $m_{\gamma\gamma}$ distribution and reduces the continuum background.

In Tables 2 and 3 we show our results obtained from the cut-based analysis. The signal strength depends strongly on m_H , $\sin\theta$ and $\text{BR}(H \rightarrow A_H A_H)$. For these we choose the benchmark values $\sin\theta=0.3$, $\text{BR}(H \rightarrow A_H A_H) = 1.0$ and 0.7 in order to maximize the event rate, while m_H is taken to be 500 GeV and above. For lower m_H , the existing LHC data already constrain the model as we show in the subsequent section. Hence, $m_H \geq 500$ GeV represents the range of interest for the future LHC runs, as long as $\sin\theta$ and $\text{BR}(H \rightarrow A_H A_H)$ are relatively large. To paint a more complete picture, in Section 3.4.1 we discuss the LHC reach in terms of m_H leaving $\text{BR}(H \rightarrow A_H A_H)$ as a free parameter.

Cuts **C2**, **C3** and **C5** prove to be the most effective ones in reducing the background. Clearly, the combined impact of the chosen cuts is adequate for our purposes, yet they also decrease the signal cross-section to the extent that any possible signal could only be observed at high-luminosity LHC. The 14 TeV LHC is projected to accumulate an integrated luminosity of 3000 fb^{-1} , which appears insufficient to obtain even 3σ statistical significance in most of the parameter space.⁶ We have also tried to soften the cuts to increase the signal rate, but that eventually results in a worse signal to background ratio. The best case scenario here is BP1, for which the significance factor at 3000 fb^{-1} is $\sim 2.5\sigma$ if we assume $\sigma_B = 0$. Therefore, our conclusion is that imposing rectangular cuts does not lead to good discovery prospects.

⁶We use the following definition of statistical significance: $\mathcal{S} = S/\sqrt{S+B+\sigma_B^2}$, where S and B are the number of signal and background events, respectively, and the background uncertainty is taken to be negligibly small, $\sigma_B \ll B$.

Channels	Production cross-section (fb)	Cross-section after cuts (fb)
$t\bar{t}h(h \rightarrow \gamma\gamma)$	0.673	2.2×10^{-4}
$b\bar{b}h(h \rightarrow \gamma\gamma)$	0.164	6.4×10^{-6}
$Zh(Z \rightarrow b\bar{b}, h \rightarrow \gamma\gamma)$	0.141	—
$\gamma\gamma + \text{jets}$	61660.7	—
$t\bar{t}\gamma\gamma$	2457.6	2.4×10^{-3}
$b\bar{b}\gamma\gamma$	5144.41	—
$ZZ(\rightarrow \nu\bar{\nu}b\bar{b}) + \text{photons}$	2.106	—
$b\bar{b}\gamma + \text{jets}$	9.76×10^6	—
$b\bar{b} + \text{jets}$	7.74×10^9	—

Table 2: The SM background channels along with their cross-sections before and after the cuts. Numerically negligible results are not shown. Here we have used a flat rate of 0.1% for the probability of a jet being mistagged as a photon.

3.3 Multivariate analysis

Evidently, the cut-based analysis is not sensitive enough to probe the present scenario at the 14 TeV LHC even at high luminosity. Thus, we next explore the possibility of improving the analysis with machine learning techniques, namely the Gradient Boosted Decision Trees (BDT) [59]. This method of data analysis is being used quite extensively in LHC searches to good effect [24, 60–64]. We have chosen the XGBoost [59] toolkit for the gradient boosting analysis. Below we list the kinematic variables used in the decision trees (cf. [43]).

1. Number of b -jets, N_b .
2. Number of photons, N_γ .
3. Transverse momentum of the hardest b -jet, $p_T^{b_1}$.
4. Transverse momentum of the second hardest b -jet, $p_T^{b_2}$.
5. Transverse momentum of the hardest photon, $p_T^{\gamma_1}$.
6. Transverse momentum of the second hardest photon, $p_T^{\gamma_2}$.
7. Missing transverse energy, \cancel{E}_T .
8. Invariant mass of the hardest b -pair, $M_{\text{inv}}^{b\bar{b}}$.
9. Invariant mass of the hardest photon pair, $M_{\text{inv}}^{\gamma\gamma}$.
10. Effective mass, M_{eff} , defined as the scalar sum of the transverse momenta of the jets, photons and \cancel{E}_T .
11. Angular separation between the $b\bar{b}$ pair and the photon pair, $\Delta\phi(b\bar{b}, \gamma\gamma)$.
12. Ratio of the hardest photon p_T and di-photon invariant mass, $R_1 = \frac{p_T^{\gamma_1}}{M_{\text{inv}}^{\gamma\gamma}}$.
13. Ratio of the second hardest photon p_T and di-photon invariant mass, $R_2 = \frac{p_T^{\gamma_2}}{M_{\text{inv}}^{\gamma\gamma}}$.

We have chosen 1000 trees, maximum depth 4 and learning rate 0.01 for our analysis. We combine data on the above kinematic variables for our signal events with all the background events in one data file. All the events are required to have at least two b -jets ($p_T^b > 25$ GeV), at least two photons ($p_T^\gamma > 20$ GeV) and no charged leptons with $p_T > 20$ GeV. We have combined the background events after properly weighting them according to their cross-sections subject to these cuts. As a result, more importance is given to the dominant backgrounds while training the data. We also make sure that there are enough signal events to match the total weight of the background events.

Benchmark Points	Production cross-section (fb)	Cross-section after cuts (fb)
BP1: $m_H = 500 \text{ GeV}, m_{A_H} = 240 \text{ GeV}, m_{A_L} = 10 \text{ GeV}$ BP2: $m_H = 500 \text{ GeV}, m_{A_H} = 240 \text{ GeV}, m_{A_L} = 100 \text{ GeV}$	0.640 (0.448)	3.66×10^{-3} (2.56×10^{-3}) 3.05×10^{-3} (2.14×10^{-3})
BP3: $m_H = 600 \text{ GeV}, m_{A_H} = 280 \text{ GeV}, m_{A_L} = 10 \text{ GeV}$ BP4: $m_H = 600 \text{ GeV}, m_{A_H} = 280 \text{ GeV}, m_{A_L} = 150 \text{ GeV}$	0.286 (0.200)	9.25×10^{-4} (6.48×10^{-4}) 8.95×10^{-4} (6.27×10^{-4})
BP5: $m_H = 700 \text{ GeV}, m_{A_H} = 340 \text{ GeV}, m_{A_L} = 10 \text{ GeV}$ BP6: $m_H = 700 \text{ GeV}, m_{A_H} = 340 \text{ GeV}, m_{A_L} = 200 \text{ GeV}$	0.133 (0.093)	4.16×10^{-4} (2.91×10^{-4}) 3.33×10^{-4} (2.33×10^{-4})

Table 3: The signal cross-section $\sigma(pp \rightarrow H \rightarrow A_H A_H \rightarrow h A_L h A_L \rightarrow b \bar{b} \gamma \gamma A_L A_L)$ before and after the cuts. For all the benchmark points, $\sin\theta=0.3$, $\text{BR}(H \rightarrow A_H A_H)=1.0$ or 0.7 (in parentheses), and $\text{BR}(A_H \rightarrow A_L h)=1.0$.

We take 80% of our data for training and 20% for testing. Each of our data samples typically contains values of the kinematic variables corresponding to $\sim 10^6$ events. These include the final states subject to our conditions on b-jets, photons and charged leptons as discussed above. In order to obtain this data set, we have generated $\sim 10^7$ Monte Carlo events for the backgrounds and $\sim 10^6$ events for the signal benchmark points.

3.3.1 Results

Fig. 6 shows results of our multivariate analysis for benchmark point BP1. The BDT classifier response shows clear distinction between the signal and the background. We find that among the kinematic variables listed above, $M_{\text{inv}}^{b\bar{b}}$ and \cancel{E}_T are the two most important discriminators followed by $M_{\text{inv}}^{\gamma\gamma}$. The right panel of Fig. 6 shows the Receiver Operating Characteristic (ROC) curve for BP1. The x-axis (efficiency) indicates the fraction of identified signal events after imposing the BDT classifier while the y-axis (Purity) indicates the ratio of identified signal events to the total number of identified events (signal plus background) after imposing the classifier. The area under the curve (AUC) is a good indicator of the BDT performance. For this benchmark point, $\text{AUC}=0.90$.

Our multivariate analysis results are quite promising and prove to be a significant improvement over those for the cut-based analysis. The AUC indicator is close to 0.9 for all the benchmark points, which shows that the BDT classifier is efficient in distinguishing the signal from the background in all considered cases. In Table 4, we present the AUC for the benchmark points along with the required luminosity to achieve a signal significance of 3σ .

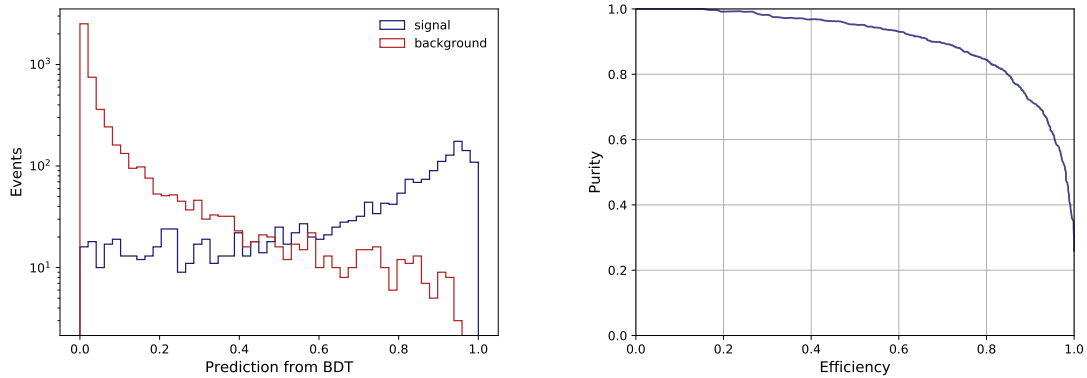


Figure 6: Example of the BDT classifier response for BP1 ($m_H = 500$ GeV, $m_{A_H} = 240$ GeV, $m_{A_L} = 10$ GeV) in differentiating the signal and background events. The ROC curve in the right panel indicates efficiency of the algorithm.

This approach allows one to constrain the low H -mass window already with the existing LHC data. The integrated luminosity required to achieve the 3σ significance for $m_H = 450$ GeV, $m_{A_H} = 150$ GeV, $\sin\theta = 0.3$ and $\text{BR}(H \rightarrow A_H A_H) = 1.0, 0.7$ is 72 and 114 fb^{-1} , respectively. Thus, the current set of 139 fb^{-1} of data collected should be sufficient to exclude $m_H \leq 450$ GeV for these parameter values, although the $2b + 2\gamma + \cancel{E}_T$ channel has not yet been analyzed by ATLAS and CMS. This justifies our choice of the m_H benchmark values of 500 GeV and above for the future LHC runs.

From our BDT analysis, we conclude that 9 out of the 13 kinematic variables used are essential to obtain the sensitivity indicated in Table 4. The four less essential variables are N_b , N_γ , R_1 and R_2 . Among these, N_b and N_γ are rendered inconsequential by the criteria we have set to select the final states, which ensure that all the signal and background events already have at least one pair of b-jets and photons. Some of the important kinematic variables, specifically $p_T^{\gamma_1}$, $p_T^{\gamma_2}$ and $M_{\text{inv}}^{\gamma\gamma}$, ensure that R_1 and R_2 are not essential either. With the remaining 9 variables, we have performed a 10-fold cross validation check in order to assess the robustness of our analysis. We have randomly split our data set in train and test sets of similar size and computed the signal significance for 10 such different combinations. In Table 5, we present the

Benchmark points	Area under the ROC curve	Required luminosity (fb^{-1})
BP1	0.89	300 (505)
BP2	0.87	707 (1264)
BP3	0.91	870 (1433)
BP4	0.88	2255 (4174)
BP5	0.91	3911 (7381)
BP6	0.88	5995 (11469)

Table 4: The area under the ROC curve for the benchmark points (see Table 3) along with the required luminosity to achieve a 3σ signal significance in the $2b + 2\gamma + \cancel{E}_T$ channel at the 14 TeV LHC assuming $\text{BR}(H \rightarrow A_H A_H) = 1$ or 0.7 (in parentheses).

Significance factors	Mean	Variance
0.171, 0.174, 0.172, 0.168, 0.175, 0.171, 0.176, 0.178, 0.169, 0.172	0.1726	3.0×10^{-3}

Table 5: Significance factors, their mean and their variance obtained in our 10-fold validation procedure for $2b + 2\gamma + \cancel{E}_T$ at BP1. The integrated luminosity is taken to be 1 fb^{-1} .

resulting signal significance factors obtained at an integrated luminosity of 1 fb^{-1} along with the corresponding mean and the variance for the benchmark point BP1. The variance is clearly quite small, indicating the robustness of our results.

3.4 Multivariate analysis for $2b\text{-jets} + 2\ell + \cancel{E}_T$ in the final state

Another promising channel for the di-Higgs and dark matter search is provided by the $\bar{b}b$ and WW^* decay modes of the Higgs bosons. Tagging on leptonic decays of the W 's, one obtains a clean final state with $2b\text{-jets} + 2\ell + \cancel{E}_T$. Here we take $\ell = e, \mu$. The challenge is to suppress the $t\bar{t} + \text{jets}$ background which has a much larger cross-section. Further background contributions come from the $t\bar{t}V$, $t\bar{t}h$, VVV and $VV + \text{jets}$ ($V \equiv W^\pm, Z$) channels. We perform a multivariate analysis of our signal with the following kinematic variables (cf. [65]):

1. Number of b -jets, N_b .
2. Number of charged leptons (e or μ), N_ℓ .
3. Number of non- b -tagged jets, N_j .
4. Transverse momentum of the hardest b -jet, $p_T^{b_1}$.
5. Transverse momentum of the second hardest b -jet, $p_T^{b_2}$.
6. Transverse momentum of the hardest charged lepton, $p_T^{\ell_1}$.
7. Transverse momentum of the second hardest charged lepton, $p_T^{\ell_2}$.
8. Missing transverse energy, \cancel{E}_T .
9. Effective mass defined as a scalar sum of the transverse momenta of the b -jets, leptons and \cancel{E}_T .
10. Invariant mass of the b -jet pair, $m_{\text{inv}}^{b\bar{b}}$.
11. Invariant mass of the lepton pair, $m_{\text{inv}}^{\ell\bar{\ell}}$.
12. Transverse momentum of the dilepton system, $p_T^{\ell\bar{\ell}}$.
13. Transverse momentum of the b -jet pair, $p_T^{b\bar{b}}$.
14. Separation between the two charged leptons, $\Delta R^{\ell\bar{\ell}}$.
15. Separation between the two b -jets, $\Delta R^{b\bar{b}}$.
16. Azimuthal separation between the b -jet pair and the dilepton system, $\Delta\phi(b\bar{b}, \ell\bar{\ell})$.

3.4.1 Results

We collect information on these kinematic variables subject to the following preliminary cuts: the final state is required to have at least two b -jets with $p_T > 25 \text{ GeV}$, at least two charged leptons with $p_T > 20 \text{ GeV}$ and $\cancel{E}_T > 50 \text{ GeV}$. The final results are summarised in Table 6. In Fig. 7, we present the required integrated luminosity for a 3σ signal significance in both channels.

Apart from N_b and N_ℓ , all the kinematic variables are essential with $m_{\text{inv}}^{b\bar{b}}$, \cancel{E}_T , $m_{\text{inv}}^{\ell\bar{\ell}}$ and $\Delta R^{b\bar{b}}$ being the most important ones. We have performed a 10-fold cross validation

Benchmark Points	Area under the ROC curve	Required Luminosity (fb^{-1})
BP1	0.88	463 (900)
BP2	0.87	819 (1614)
BP3	0.85	2900 (5804)
BP4	0.83	11468 (23192)

Table 6: The area under the ROC curve for the benchmark points (see Table 3) along with the required integrated luminosity to achieve a 3σ signal significance in the $2b + 2\ell + \cancel{E}_T$ at the 14 TeV LHC assuming $\text{BR}(H \rightarrow A_H A_H)=1$ or 0.7 (in parentheses). BP5 and BP6 require very large integrated luminosity and thus not shown.

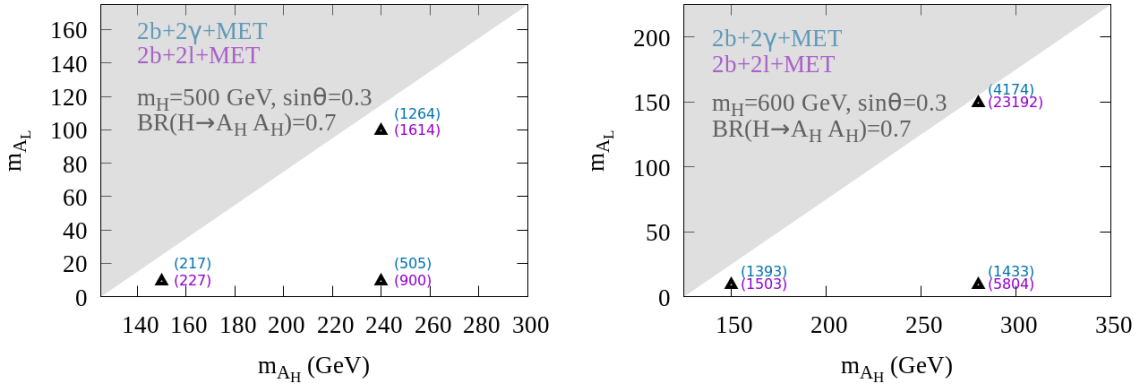


Figure 7: Integrated luminosity required for a 3σ signal significance in the $2b + 2\gamma + \cancel{E}_T$ and $2b + 2\ell + \cancel{E}_T$ channels at 14 TeV LHC.

check for this analysis as well following the prescription of Section 3.3.1. In Table 7, we present the resulting 10 signal significance factors obtained at an integrated luminosity of 1 fb^{-1} along with the corresponding mean and the variance for the benchmark point BP1. The variance is sufficiently small indicating robustness of our results.

The results can also be presented in terms of the exclusion limits on the model. In particular, the branching ratio for the decay $H \rightarrow A_H A_H$ can be severely constrained with 3ab^{-1} of data. Fig. 8 displays the corresponding bound for a representative set of parameters, namely $m_{A_H} = 150 \text{ GeV}$, $m_{A_L} = 10 \text{ GeV}$ and $\sin\theta = 0.2, 0.3$. The constraint can be as strong as $\text{BR}(H \rightarrow A_H A_H) < 7\%$ for $m_H < 400 \text{ GeV}$. Substantial values of $\text{BR}(H \rightarrow A_H A_H)$ can be probed up to $m_H \sim 600 - 700 \text{ GeV}$. We also see that the $2b + 2\gamma + \cancel{E}_T$ channel performs slightly better than $2b + 2\ell + \cancel{E}_T$ does.

Significance factors	Mean	Variance
0.143, 0.144, 0.140, 0.138, 0.143, 0.137, 0.136, 0.136, 0.139, 0.138	0.1394	2.8×10^{-3}

Table 7: Significance factors, their mean and their variance obtained in our 10-fold validation procedure for $2b + 2\ell + \cancel{E}_T$ at BP1. The integrated luminosity is taken to be 1 fb^{-1} .

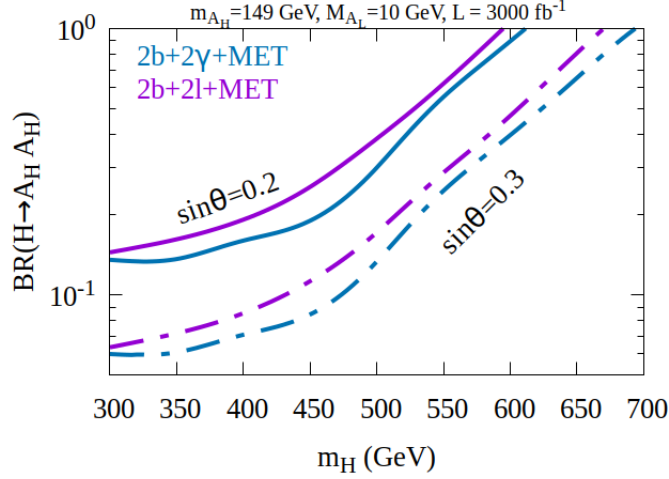


Figure 8: 3σ sensitivity of the $2b+2\gamma+\cancel{E}_T$ and $2b+2\ell+\cancel{E}_T$ channels to $\text{BR}(H \rightarrow A_H A_H)$ at 14 TeV LHC with integrated luminosity of 3000 fb^{-1} . The dashed (solid) line corresponds to $\sin\theta = 0.3$ ($\sin\theta = 0.2$).

So far, we have presented our results assuming $\sigma_B \simeq 0$. It is very difficult to forecast the future background uncertainty, so we have to resort to simple estimates. Let us assume the background uncertainty to be 20% of the total background, i.e., $\sigma_B = 0.2 \times B$. Consequently, σ_B^2 can be very large for signal regions with a large background cross-section. The $2b+2\ell+\cancel{E}_T$ signal is thus affected quite severely since $t\bar{t} + \text{jets}$ is a direct background to this final state and it comes with a large irreducible cross-section. We find that at 3000 fb^{-1} luminosity with the parameter choices shown in Fig. 8, the signal significance for the $2b+2\gamma+\cancel{E}_T$ final state reduces by a factor of ~ 2 when $\sigma_B = 0.2 \times B$ compared to the case with $\sigma_B = 0$, whereas for $2b+2\ell+\cancel{E}_T$ it reduces by ~ 10 . Since at such high luminosity, $\mathcal{S} = S/\sqrt{S+B+\sigma_B^2} \simeq S/\sqrt{B+\sigma_B^2}$, the required $\text{BR}(H \rightarrow A_H A_H)$ in the $2b+2\gamma+\cancel{E}_T$ and $2b+2\ell+\cancel{E}_T$ final states have to be scaled up by factors of 2 and 10, respectively. The scale factor remains the same for the different choices of $\sin\theta$ since the kinematics of the final state are not affected.

4 LHC search for a tri-Higgs and dark matter final state

4.1 Multivariate analysis for $\geq 3b\text{-jets} + 2\ell + \cancel{E}_T$ in the final state

In the presence of additional heavy particles in the dark sector, more exotic final states can be produced. In particular, cascade decays can lead to 3 or more Higgs bosons h in the final state. For example, the heavy Higgs H can produce a pair of heavy A'_H , which in turn decay via two different decay modes $A'_H \rightarrow A_H h$ and $A'_H \rightarrow A_L h$. Subsequently, A_H decays into A_L and h , thereby generating a multi-Higgs final state. The channel with four Higgs bosons suffers from severe kinematic suppression, while the tri-Higgs one could potentially be interesting.

Multi-Higgs production can be efficient if the decays happen on-shell. This implies

that A'_H must be heavier than 250 GeV and thus $m_H > 500$ GeV. Given a tri-Higgs final state, there are a number of options to consider for Higgs decay. If all three decay into $\bar{b}b$ pairs, the signal extraction is marred by a large QCD multi-jet background and possible misidentification of light flavor jets as b -jets. For the current study, we choose instead 2 $\bar{b}b$ pairs and leptonically decaying WW^* as our final state. It has the advantage of being relatively clean and, in addition, we may recycle many of the background calculations done in the previous section. We perform a multivariate analysis with the following kinematic variables:

1. Number of b -jets, N_b .
2. Number of charged leptons (e or μ), N_ℓ .
3. Number of non- b -tagged jets, N_j .
4. Transverse momentum of the hardest b -jet, $p_T^{b_1}$, involved in a b -jet pair with $m_{\text{inv}}^{b\bar{b}}$ closest to 125 GeV.
5. Transverse momentum of the second hardest b -jet, $p_T^{b_2}$, involved in a b -jet pair with $m_{\text{inv}}^{b\bar{b}}$ closest to 125 GeV.
6. Transverse momentum of the hardest charged lepton, $p_T^{\ell_1}$.
7. Transverse momentum of the second hardest charged lepton, $p_T^{\ell_2}$.
8. Missing transverse energy, \cancel{E}_T .
9. Effective mass, defined as a scalar sum of the transverse momenta of the b -jets, leptons and \cancel{E}_T .
10. Invariant mass of the b -jet pair, $m_{\text{inv}}^{b_1 b_2}$.
11. Invariant mass of the lepton pair, $m_{\text{inv}}^{\ell\bar{\ell}}$.
12. Transverse momentum of the dilepton system, $p_T^{\ell\bar{\ell}}$.
13. Transverse momentum of the b -jet pair, $p_T^{b_1 b_2}$.
14. Separation between the two charged leptons, $\Delta R^{\ell\bar{\ell}}$.
15. Separation between the two b -jets, $\Delta R^{b_1 b_2}$.
16. Azimuthal separation between the b -jet pair and the dilepton system, $\Delta\phi(b_1 b_2, \ell\bar{\ell})$.

We collect information on these kinematic variables imposing the following preliminary cuts: the final state is required to have at least 3 b -jets with $p_T > 25$ GeV and at least two charged leptons with $p_T > 20$ GeV. We construct all possible b -jet pairs in the final state, compute the corresponding invariant masses, and then identify the pair that has $m_{\text{inv}}^{b\bar{b}}$ closest to 125 GeV. We call the harder b -jet in this pair b_1 and the other one is identified as b_2 .

Note that we are not using the third b -jet kinematics directly in our multivariate analysis. Including it adds a few more variables to the list: $p_{b_3}^T$, $\Delta\phi(b_3, \ell\bar{\ell})$ and $\Delta\phi(b_1 b_2, b_3)$. However, we have verified that these do not improve our results.

The sensitivity of this signal region is weaker compared to the previous two. Although the BDT classifier is quite efficient in isolating the signal events, the few remaining background events have a large enough cross-section to suppress the signal significance. This is due to the small signal cross-section to start with, which is further reduced by detector simulations and applying the BDT classifier.

To give an example, consider the parameter set $m_H = 600$ GeV, $m_{A'_H} = 290$ GeV, $m_{A_H} = 150$ GeV, $m_{A_L} = 20$ GeV. The production cross section for the required final state is 0.107 fb. Optimizing the signal to background ratio using our multivariate analysis, we find that the 1σ signal significance is achieved with 3000 fb^{-1} integrated luminosity, while that at 2σ level requires 12000 fb^{-1} . Clearly, this is beyond the reach of the LHC.

Although our result for the $3b\text{-jets} + 2\ell + \cancel{E}_T$ channel is negative, a fully $b\text{-jet} + \cancel{E}_T$ final state may be more promising. It requires a dedicated analysis which we reserve for future work.

5 Summary and Conclusions

In this work, we have considered dark sectors with spontaneously broken gauge symmetries, where dark cascade decays naturally lead to multi-Higgs final states with missing energy. We have introduced a simplified model which captures main features of realistic hidden sectors containing dark matter as well as further heavier states.

The focus of this work is 2 and 3 Higgs final states which subsequently decay into $\bar{b}b, \gamma\gamma$ and WW . Using multivariate analysis with Boosted Decision Trees, we find that the $2b + 2\gamma + \cancel{E}_T$ and $2b + 2\ell + \cancel{E}_T$ channels are promising in the context of 14 TeV LHC with 3 ab^{-1} integrated luminosity. In particular, light dark matter A_L with mass $\lesssim 100 \text{ GeV}$ can be probed efficiently for the dark Higgs (H) mass below 700 GeV and its mixing angle with the SM Higgs $\sin \theta \sim 0.2 - 0.3$. In this region, 3σ and higher signal significance can be achieved. The result can also be translated into a bound on the dark Higgs decay into the heavier partners of dark matter A_H , with sensitivity to $\text{BR}(H \rightarrow A_H A_H)$ reaching 6% in the best case scenario.

The 3 Higgs final state, on the other hand, appears far less promising, at least for the decay channels considered. Fully hadronic Higgs decays may change this situation, but require a dedicated background study and detection simulation.

Acknowledgements

M.F. is supported by the National Research Foundation of South Africa - The World Academy of Sciences (NRF-TWAS) Grant No. 110790, Reference No. SFH170609238739. C.G. is supported by the European Research Council grant NEO-NAT.

References

- [1] V. Silveira and A. Zee, Phys. Lett. **161B**, 136 (1985).
- [2] R. M. Schabinger and J. D. Wells, Phys. Rev. D **72**, 093007 (2005) [hep-ph/0509209].
- [3] B. Patt and F. Wilczek, hep-ph/0605188.
- [4] B. Di Micco *et al.*, arXiv:1910.00012 [hep-ph].
- [5] K. T. Matchev and S. D. Thomas, Phys. Rev. D **62** (2000) 077702 [hep-ph/9908482].
- [6] Z. Kang, P. Ko and J. Li, Phys. Rev. Lett. **116** (2016) no.13, 131801 [arXiv:1504.04128 [hep-ph]].
- [7] S. M. Etesami and M. Mohammadi Najafabadi, Phys. Rev. D **92** (2015) no.7, 073013 [arXiv:1505.01028 [hep-ph]].
- [8] A. Papaefstathiou and K. Sakurai, JHEP **1602** (2016) 006 [arXiv:1508.06524 [hep-ph]].
- [9] X. F. Han, L. Wang and J. M. Yang, Mod. Phys. Lett. A **31** (2016) no.31, 1650178 [arXiv:1509.02453 [hep-ph]].

- [10] Z. Kang, P. Ko and J. Li, Phys. Rev. D **93** (2016) no.7, 075037 [arXiv:1512.08373 [hep-ph]].
- [11] S. Biswas, E. J. Chun and P. Sharma, JHEP **1612** (2016) 062 [arXiv:1604.02821 [hep-ph]].
- [12] I. Brivio, M. B. Gavela, L. Merlo, K. Mimasu, J. M. No, R. del Rey and V. Sanz, Eur. Phys. J. C **77** (2017) no.8, 572 [arXiv:1701.05379 [hep-ph]].
- [13] E. Arganda, J. L. Díaz-Cruz, N. Mileo, R. A. Morales and A. Szyrkman, Nucl. Phys. B **929** (2018) 171 [arXiv:1710.07254 [hep-ph]].
- [14] C. R. Chen, Y. X. Lin, H. C. Wu and J. Yue, arXiv:1804.00405 [hep-ph].
- [15] E. Bernreuther, J. Horak, T. Plehn and A. Butter, SciPost Phys. **5** (2018) no.4, 034 [arXiv:1805.11637 [hep-ph]].
- [16] A. Titterton, U. Ellwanger, H. U. Flaecher, S. Moretti and C. H. Shepherd-Themistocleous, JHEP **1810** (2018) 064 [arXiv:1807.10672 [hep-ph]].
- [17] S. Banerjee, B. Batell and M. Spannowsky, Phys. Rev. D **95**, no.3, 035009 (2017) doi:10.1103/PhysRevD.95.035009 [arXiv:1608.08601 [hep-ph]].
- [18] S. Banerjee, F. Krauss and M. Spannowsky, Phys. Rev. D **100**, 073012 (2019) doi:10.1103/PhysRevD.100.073012 [arXiv:1904.07886 [hep-ph]].
- [19] A. Adhikary, S. Banerjee, R. Kumar Barman and B. Bhattacharjee, JHEP **09**, 068 (2019) doi:10.1007/JHEP09(2019)068 [arXiv:1812.05640 [hep-ph]].
- [20] S. Banerjee, C. Englert, M. L. Mangano, M. Selvaggi and M. Spannowsky, Eur. Phys. J. C **78**, no.4, 322 (2018) doi:10.1140/epjc/s10052-018-5788-y [arXiv:1802.01607 [hep-ph]].
- [21] A. M. Sirunyan *et al.* [CMS Collaboration], Phys. Rev. D **97** (2018) no.3, 032007 [arXiv:1709.04896 [hep-ex]].
- [22] A. M. Sirunyan *et al.* [CMS Collaboration], Phys. Rev. Lett. **120** (2018) no.24, 241801 [arXiv:1712.08501 [hep-ex]].
- [23] M. Aaboud *et al.* [ATLAS Collaboration], Phys. Rev. D **98** (2018) no.9, 092002 [arXiv:1806.04030 [hep-ex]].
- [24] M. Blanke, S. Kast, J. M. Thompson, S. Westhoff and J. Zurita, JHEP **1904** (2019) 160 [arXiv:1901.07558 [hep-ph]].
- [25] J. S. Kim, O. Lebedev and D. Schmeier, JHEP **1511** (2015) 128 [arXiv:1507.08673 [hep-ph]].
- [26] C. Gross, O. Lebedev and Y. Mambrini, JHEP **1508**, 158 (2015) [arXiv:1505.07480 [hep-ph]].
- [27] T. Hambye, JHEP **0901**, 028 (2009) [arXiv:0811.0172 [hep-ph]].
- [28] O. Lebedev, H. M. Lee and Y. Mambrini, Phys. Lett. B **707**, 570 (2012) [arXiv:1111.4482 [hep-ph]].
- [29] D. Buttazzo, L. Di Luzio, G. Landini, A. Strumia and D. Teresi, JHEP **1910** (2019) 067 [arXiv:1907.11228 [hep-ph]].
- [30] D. Buttazzo, L. Di Luzio, P. Ghorbani, C. Gross, G. Landini, A. Strumia, D. Teresi and J. W. Wang, arXiv:1911.04502 [hep-ph].
- [31] A. Karam and K. Tamvakis, Phys. Rev. D **94**, no. 5, 055004 (2016) [arXiv:1607.01001 [hep-ph]].
- [32] A. Poulin and S. Godfrey, Phys. Rev. D **99**, no. 7, 076008 (2019) [arXiv:1808.04901 [hep-ph]].

- [33] G. Arcadi, C. Gross, O. Lebedev, S. Pokorski and T. Toma, Phys. Lett. B **769**, 129 (2017) [arXiv:1611.09675 [hep-ph]].
- [34] G. Arcadi, C. Gross, O. Lebedev, Y. Mambrini, S. Pokorski and T. Toma, JHEP **1612** (2016) 081 [arXiv:1611.00365 [hep-ph]].
- [35] K. Huitu, N. Koivunen, O. Lebedev, S. Mondal and T. Toma, Phys. Rev. D **100**, no. 1, 015009 (2019) [arXiv:1812.05952 [hep-ph]].
- [36] A. Falkowski, C. Gross and O. Lebedev, JHEP **1505**, 057 (2015) [arXiv:1502.01361 [hep-ph]].
- [37] T. Robens and T. Stefaniak, Eur. Phys. J. C **75**, 104 (2015) doi:10.1140/epjc/s10052-015-3323-y [arXiv:1501.02234 [hep-ph]].
- [38] A. Djouadi, O. Lebedev, Y. Mambrini and J. Quevillon, Phys. Lett. B **709**, 65 (2012) [arXiv:1112.3299 [hep-ph]].
- [39] A. Djouadi, A. Falkowski, Y. Mambrini and J. Quevillon, Eur. Phys. J. C **73**, no. 6, 2455 (2013) [arXiv:1205.3169 [hep-ph]].
- [40] C. H. Chen and T. Nomura, Phys. Rev. D **93**, no. 7, 074019 (2016) [arXiv:1507.00886 [hep-ph]].
- [41] A. Adhikary, S. Banerjee, R. K. Barman, B. Bhattacharjee and S. Niyogi, JHEP **1807**, 116 (2018) [arXiv:1712.05346 [hep-ph]].
- [42] A. Alves, T. Ghosh and F. S. Queiroz, Phys. Rev. D **100** (2019) no.3, 036012 [arXiv:1905.03271 [hep-ph]].
- [43] A. M. Sirunyan *et al.* [CMS Collaboration], Phys. Lett. B **788**, 7 (2019) [arXiv:1806.00408 [hep-ex]].
- [44] ATLAS Collaboration, ATL-PHYS-PUB-2016-026.
- [45] J. Alwall, M. Herquet, F. Maltoni, O. Mattelaer and T. Stelzer, JHEP **1106**, 128 (2011) [arXiv:1106.0522 [hep-ph]].
- [46] J. Alwall *et al.*, JHEP **1407**, 079 (2014) [arXiv:1405.0301 [hep-ph]].
- [47] R. D. Ball *et al.*, Nucl. Phys. B **867**, 244 (2013) [arXiv:1207.1303 [hep-ph]].
- [48] R. D. Ball *et al.* [NNPDF Collaboration], JHEP **1504**, 040 (2015) [arXiv:1410.8849 [hep-ph]].
- [49] T. Sjostrand, S. Mrenna and P. Z. Skands, JHEP **0605**, 026 (2006) [hep-ph/0603175].
- [50] T. Sjostrand *et al.*, Comput. Phys. Commun. **191**, 159 (2015) [arXiv:1410.3012 [hep-ph]].
- [51] S. Hoeche, F. Krauss, N. Lavesson, L. Lonnblad, M. Mangano, A. Schalicke and S. Schumann, hep-ph/0602031.
- [52] M. L. Mangano, M. Moretti, F. Piccinini and M. Treccani, JHEP **0701**, 013 (2007) [hep-ph/0611129].
- [53] J. de Favereau *et al.* [DELPHES 3 Collaboration], JHEP **1402**, 057 (2014) [arXiv:1307.6346 [hep-ex]].
- [54] M. Selvaggi, J. Phys. Conf. Ser. **523**, 012033 (2014).
- [55] A. Mertens, J. Phys. Conf. Ser. **608**, no. 1, 012045 (2015).
- [56] M. Cacciari, G. P. Salam and G. Soyez, Eur. Phys. J. C **72**, 1896 (2012) [arXiv:1111.6097 [hep-ph]].
- [57] M. Cacciari, G. P. Salam and G. Soyez, JHEP **0804**, 063 (2008) [arXiv:0802.1189 [hep-ph]].

- [58] ATLAS Collaboration, ATL-PHYS-PUB-2015-022.
- [59] T. Chen and C. Guestrin, arXiv:1603.02754 [cs.LG].
- [60] P. Baldi, P. Sadowski and D. Whiteson, Nature Commun. **5**, 4308 (2014) [arXiv:1402.4735 [hep-ph]].
- [61] K. Y. Oyulmaz, A. Senol, H. Denizli and O. Cakir, Phys. Rev. D **99**, no. 11, 115023 (2019) [arXiv:1902.03037 [hep-ph]].
- [62] B. Bhattacharjee, S. Mukherjee and R. Sengupta, arXiv:1904.04811 [hep-ph].
- [63] N. Bakhiet, M. Y. Khlopov and T. Hussein, arXiv:1507.06547 [hep-ph].
- [64] R. D. Field, Y. Kanev, M. Tayebnejad and P. A. Griffin, Phys. Rev. D **53**, 2296 (1996).
- [65] G. Aad *et al.* [ATLAS Collaboration], arXiv:1908.06765 [hep-ex].